Magnetic Resonance Imaging 59 (2019) 97–104

Contents lists available at ScienceDirect

Magnetic Resonance Imaging

journal homepage: www.elsevier.com/locate/mri

Case report

Feasibility study of a double resonant 8-channel ^{1}H/ 8-channel ^{23}Na receive-only head coil at 3 Tesla

Matthias Malzacher*, Jorge Chacon-Caldera, Nadia Paschke, Lothar R. Schad

Computer Assisted Clinical Medicine, Medical Faculty Mannheim, Heidelberg University, Mannheim, Germany

ARTICLE INFO

Keywords:
Sodium MRI
Rx arrays
Double resonant coils
Parallel imaging

ABSTRACT

Sodium (^{23}Na) magnetic resonance imaging (MRI), especially brain applications are increasingly interesting since sodium MRI can provide additional information about tissue viability and vitality. In order to include sodium MRI in the clinical routine, a single RF setup is preferable which provides high sodium sensitivity and full proton performance in terms of signal-to-noise ratio (SNR) and parallel imaging performance. The aim of this work was to evaluate the feasibility of a double resonant receive (Rx) coil array for proton and sodium head MRI. The coil was designed to provide high sodium SNR and full proton performance comparable to commercial coils which are optimized for sodium MRI or for proton MRI, respectively. A measurement setup was built which comprised an 8-channel Rx degenerate Birdcage for sodium imaging and an 8-channel Rx array for proton imaging. The performance of the coil was evaluated against commercial sodium and proton coils using phantom and *in-vivo* measurements of two healthy volunteers.

1. Introduction

Sodium (^{23}Na) magnetic resonance imaging could be used by clinicians as an additional diagnostic tool next to conventional proton MRI. Besides different applications in the body [1–4], brain applications [5] are especially increasingly interesting since sodium MRI can give additional information about tissue viability and vitality [6–9]. Previous studies dealt for example with stroke [10,11], brain tumor [12,13], Alzheimer [14] or multiple sclerosis [15–17].

Nevertheless, sodium MRI is challenging due to its fast relaxation times and low MR sensitivity (approximately 10,000 times lower compared to proton (^{1}H) *in-vivo*). In order to overcome these challenges, the use of special sequences [18–20], post-processing techniques [3,21,22] and dedicated radio frequency (RF) setups [23] is crucial. A commonly used technique for homogeneous excitation and high receiver sensitivity is the transmit-only receive-only (ToRo) approach [24] which has been shown to be feasible for different sodium RF setups in previous works [25–28].

In general sodium MRI can be included in the clinical routine using a single resonant ^{23}Na coil. This coil can be realized as a transmit-receive (TxRx) coil or a ToRo setup composed of a separate transmit (Tx) and a separate receive (Rx) coil. The sodium coil can be used in combination with the systems ^{1}H body coil for registration to proton MRI. In the same way also a double resonant ^{1}H/^{23}Na coil can be used. Anyway, in order to perform different relevant clinical ^{1}H protocols (*e.g.* T_1 weighted, T_2 weighted, diffusion tensor imaging, time-of-flight *etc.*) proton coils with high SNR and good parallel imaging performance are needed in order to reduce scan time. In case of a single resonant sodium setup or a double resonant setup which cannot provide full ^{1}H performance, a coil exchange is needed which increases total measurement time and decreases patient comfort.

Many different approaches for a double resonant coil setup have been presented before [25,26,28–33]. These setups focused on the technical innovations and the SNR performance of the non-proton coils. The proton coils in these setups were only used to perform basic morphological imaging for localization but a comparison to commercial coils in terms of parallel imaging performance was not yet presented.

The aim of this work was to build a double resonant 8-channel ^{1}H ($f_{res\ 1H}$ = 123.2 MHz)/ 8-channel ^{23}Na ($f_{res\ 23Na}$ = 32.6 MHz) receive-only head array for MRI at 3 T with high sodium sensitivity and full proton imaging performance in terms of SNR and parallel imaging performance. In order to evaluate the feasibility of such a setup, sodium SNR performance was compared to a commercially available sodium head coil. Additionally, SNR, as well as parallel imaging performance for proton imaging was evaluated against a commercially available proton Rx head array. Both comparisons were performed using

Abbreviations: MRI, magnetic resonance imaging; RF, radio frequency; SNR, signal-to-noise ratio; Tx, transmit; Rx, receive; ToRo, transmit-only receive-only; DGB, degenerate Birdcage; AP, anterior - posterior; LR, left – right; SAR, specific absorption rate

* Corresponding author at: Theodor-Kutzer-Ufer 1-3, 68167 Mannheim, Germany.
E-mail address: matthias.malzacher@medma.uni-heidelberg.de (M. Malzacher).

https://doi.org/10.1016/j.mri.2019.03.013
Received 20 August 2018; Received in revised form 9 March 2019; Accepted 13 March 2019

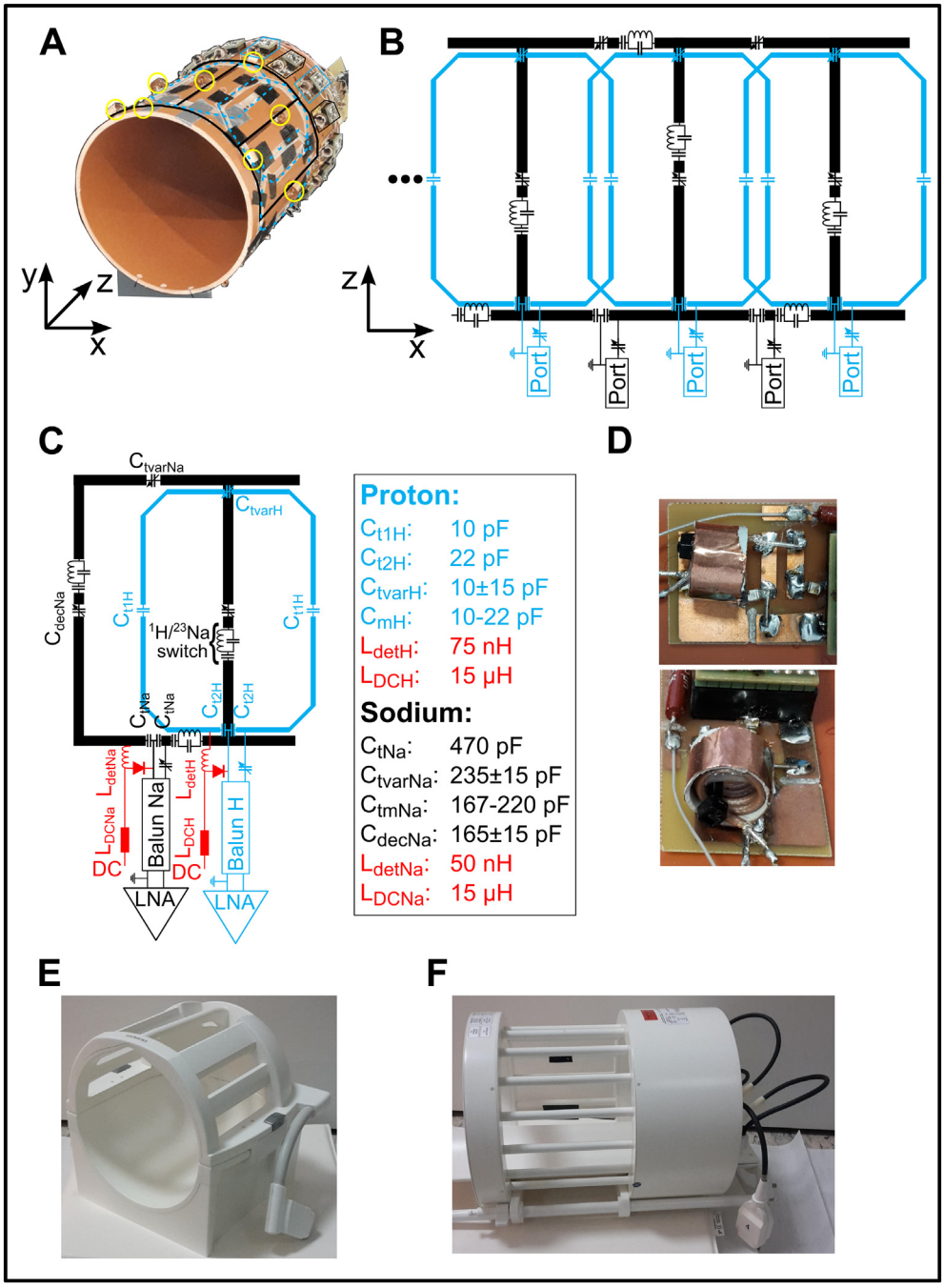

Fig. 1. A Image of the 8Rx ^{1}H/ 8Rx ^{23}Na coil. The 8Rx ^{23}Na coil is highlighted with the solid black lines and the 8Rx ^{1}H coil with the dotted blue lines. The proton traps are marked with the yellow circles. B Part of a simplified circuit diagram of the 8Rx ^{1}H/ 8Rx ^{23}Na coil with two 8Rx ^{23}Na coil elements (in black) and three 8Rx ^{1}H coil elements (in blue). C Magnified circuit diagram of a single 8Rx ^{23}Na (black) and a single 8Rx ^{1}H (blue) coil element. Sodium: C_{tNa} and C_{tvarNa} are for tuning the coil to the resonance frequency. C_{mNa} is for matching the coil and C_{decNa} is for decoupling nearest neighboring coils. L_{detNa} is for active detuning and L_{DCNa} for separating the RF and DC lines. Proton: C_{t1H}, C_{t2H} and C_{tvarH} are for tuning the coil to the resonance frequency. C_{mH} is for matching the coil. L_{detH} is for active detuning and L_{DCH} for separating the RF and DC lines. D Magnified images of an exemplary cable trap in a top and a front view. E Image of the commercial 12Rx ^{1}H coil. F Image of the commercial 1TxRx ^{1}H/^{23}Na coil. (For interpretation of the references to colour in this figure legend, the reader is referred to the web version of this article.)

phantom measurements and *in-vivo* measurements of two healthy volunteers.

2. Material and methods

2.1. Sodium array

An image of our coil is depicted in Fig. 1A. A general circuit diagram and a detailed circuit diagram are given in Fig. 1B and C. The sodium coil was built as a degenerate Birdcage (DGB) coil [34]. This structure is a conventional band-pass Birdcage [35] but the capacitors in the legs are adjusted in a way that the different modes of the Birdcage collapse. The DGB resulted in 8 independent Rx channels (8Rx ^{23}Na coil). The coil structure was made of flat copper conductor (width = 6 mm, thickness = 0.1 mm) and mounted on a PVC tube with an outer diameter of 250 mm. The dimensions of the 8Rx ^{23}Na coil elements were 98 mm in x-direction and 240 mm in z-direction (the dimensions were measured on a plane). The coil elements were split by capacitors (501 CHB JCL, Exxelia Temex, Paris, France) at four positions, two in the ring segments and two in the legs. The capacitors in the legs were used to decouple nearest neighboring coils. The capacitors in the ring segments were used to tune the individual coil elements. One of the tuning capacitors was split to generate a virtual ground. At this position the preamplifier (Stark Contrast GmbH, Erlangen, Germany) was connected *via* a capacitive matching network. A sodium cable trap (Fig. 1D) was positioned between the coil element and the preamplifier (distance to the coil 7 mm and distance to the preamplifier 15 mm). The trap was made of wound coaxial cable (RG 316C, Habia Cable GmbH, Ulm, Germany) bridged by a capacitor and shielded with copper tape. The shielding stabilized the tuning of the proton trap since it presented a

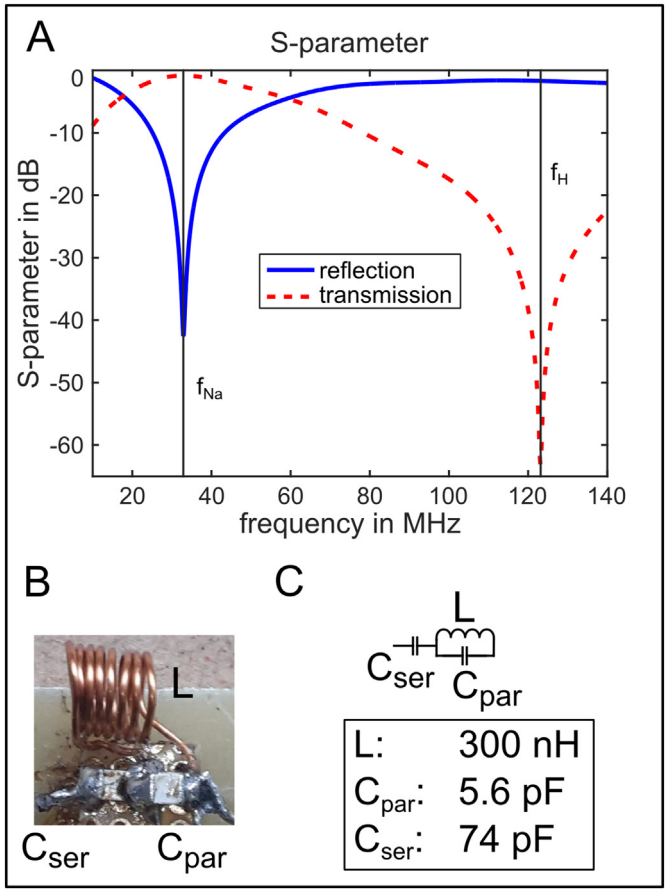

Fig. 2. A Measured S-parameters of the proton trap. The solid blue line indicates the reflection parameter and the dashed red line the transmission parameter. The sodium frequency (f_{Na}) is 32.6 MHz and the proton frequency (f_H) is 123.2 MHz. A −62.4 dB proton suppression could be found. B Image of an exemplary proton trap. C Circuit diagram of the proton trap with the respective component values. (For interpretation of the references to colour in this figure legend, the reader is referred to the web version of this article.)

steady grounding. A proton trap (Fig. 1A; Fig. 2B and C) was added to each leg and every second ring segment of the 8Rx ^{23}Na coil. This was done to avoid interactions between the sodium and the proton Rx array as well as protect the sodium Rx coil elements during the proton transmission. The two-stage trap design was chosen [36]. It comprised an inductor bridged by a capacitor and an additional capacitor in series. The inductor was made of wound enameled copper wire. The inductor value was set to 300 nH. The value of the capacitor in parallel to the inductor (C_{par}) and the capacitor in series (C_{ser}) was calculated using

$$C_{par} = \frac{1}{L\omega_{Na}^2} \tag{1}$$

$$C_{ser} = \frac{1}{L(\omega_H^2 - \omega_{Na}^2)} \tag{2}$$

with ω_{Na} being the sodium Larmor frequency and ω_H the proton Larmor frequency. This design was chosen since it presents a high impedance at the blocking (proton) frequency and a low impedance at the resonance (sodium) frequency. This avoids the need of retuning the 8Rx ^{23}Na coil element in a large scale after insertion of the trap circuit. Nevertheless, a slight frequency shift can still appear when the trap circuit is inserted.

The structure of the 8Rx ^{23}Na coil was first modeled for electromagnetic simulations (CST Computer Simulation Technology GmbH, Darmstadt, Germany) to obtain the values of the capacitors roughly. The 8Rx ^{23}Na coil was then constructed iteratively. Each coil element was first tuned to the sodium resonance frequency. Then the proton traps were added consecutively. After the insertion of a trap circuit, the resonance frequency of the coil element was readjusted to the initial resonance frequency if a frequency shift occurred. This was done by changing the value of the series capacitor of the trap circuit.

After the insertion of the traps, the coil element was decoupled from its neighbors by adjusting the capacitor in the common leg. This was done using transmission S-parameter measurements. Afterwards, each coil element was tuned and matched and preamplifier decoupling [37] was adjusted by varying the series and parallel capacitor of the matching circuit. Tuning and matching, as well as preamplifier decoupling, were optimized iteratively until both, preamplifier decoupling and tuning and matching, were adjusted. This process was repeated for each channel. Finally, all individual channels were readjusted while the other coil elements were resonant and equipped with a preamplifier.

In order to reduce SNR losses due to coil coupling, the Rx coil elements were matched in a broadband fashion [38]. The highest coupling was found between the next nearest neighboring coil elements. The two frequencies of the coupled coil elements were measured using a double pick-up loop while both coil elements are resonant (without preamplifier) and while the other coil elements are detuned [39]. The coupling coefficient k was calculated using

$$k = \frac{|f_1 - f_2|}{\sqrt{f_1 \cdot f_2}} \tag{3}$$

with f_1 the frequency of the upper mode and f_2 the frequency of the lower mode. The optimum broadband matching impedance was then calculated using

$$|z| = |1 + jkQ| \tag{4}$$

with Q the loaded Q-factor of a sodium coil element. The sodium coil elements were matched to this reflection factor at the resonance frequency with the impedance circle of the reflection S-parameter encircling the center of the smith chart [25,40].

In order to protect the Rx coil elements during transmission, an active detuning circuit was added to each coil element. This detuning circuit consisted of an inductor made of wound enameled copper wire which was placed in parallel to one of the split tuning. The inductor was adjusted in a way that it presents, together with the parallel capacitor, an open (high impedance) at the resonance frequency of the coil element which makes the coil element off-resonant. A PIN diode (MA4P7470F-1072T, MACOM GmbH, Stuttgart, Germany) was used to control this detuning circuit which was controlled by a DC signal provided by the MR system. The DC line is connected to the PIN diode using a 15 µH inductor (71.30 - M, Richard Jahre GmbH, Wilhelmshaven, Germany) to separate the AC and DC lines.

2.2. Proton array

The proton Rx array (8Rx ^{1}H coil) consisted of 8 Rx coil elements. The dimensions of the coil elements were 131 mm in x-direction and 216 mm in z-direction. The individual coil elements were decoupled using overlap decoupling. The coil elements were built in an octagonal shape to decrease capacitive coupling at the overlap positions. The coil element's size in z-direction was shorter compared to the 8Rx ^{23}Na coil to avoid large overlapping areas of the conductors. This was done to decrease capacitive coupling between the 8Rx ^{23}Na coil and the 8Rx ^{1}H coil. The geometry of the 8Rx ^{1}H coil elements in terms of overlap was found iteratively using electromagnetic simulations. In order to find the optimal overlap, two 8Rx ^{1}H coil elements were simulated with their center shifted 45° towards each other on top of the detuned sodium DGB. Both were tuned to the Larmor frequency of proton. Then the width of both coil elements was changed gradually until a decoupling of at least −15 dB was reached.

For the measurement setup the coils were made of flat copper tape

(width = 3 mm, thickness = 0.1 mm). Each coil element was split four times by a capacitor. One of the capacitors which were placed at the end of the coil element in z-direction was split to generate a virtual ground. At this point, each coil element was connected to the preamplifier (Siemens Healthcare GmbH, Erlangen, Germany) *via* a capacitive matching network. A proton cable trap was placed between the coil element and the preamplifier. The cable trap was built as described for the sodium coil elements (distance to the coil element 30 mm and distance to the preamplifier 15 mm). Each coil element was built on a flexible FR4 board (thickness = 0.2 mm) and tuned to the resonance frequency. The coil elements were placed on top of the legs of the 8Rx ^{23}Na coil (Fig. 1). The overlap distance was checked for optimum decoupling using transmission S-parameter measurements. During the mounting process the 8Rx ^{23}Na coil was detuned (as it is during the proton measurement). The optimum matching impedance for the broadband match was found as described for the 8Rx ^{23}Na coil.

Additionally, each coil element was equipped with a PIN diode driven detuning network. Finally, the elements of the 8Rx ^{23}Na coil were readjusted when needed with the proton array detuned.

2.3. Measurements

2.3.1. Phantom

All measurements were performed on a clinical 3T Tim Trio MR system (Siemens Healthcare GmbH, Erlangen, Germany). Phantom measurements were performed using a bottle shaped phantom (diameter = 115 mm, length = 205 mm) filled with 3.75 $NiSO_4x6H_2O$ + 5 g NaCl. For each SNR scan a noise measurement was performed with the same sequence parameter but without transmit power. The single channel SNR maps were combined using the matched filter approach [41]:

$$SNR = \sqrt{\sum_{ik} siSNR_i \bullet R_{ik}^{-1} \bullet siSNR_k^*} \quad (5)$$

with siSNR the single channel SNR maps and R the noise correlation matrix.

^{23}Na imaging: Sodium imaging was performed using a 3D density adapted radial sequence [19] with the following parameters: TE/TR/TA = 1 ms/100 ms/4 min, flip angle = 48°, FoV = (250 mm)^3, isotropic resolution = 6 × 6 × 6 mm^3, projections = 2500.

Flip angle adjustment was performed before each scan by increasing the pulse length of a rectangular non-selective pulse using a fixed transmit power. The pulse length was increased until the maximum signal amplitude was measured globally.

For ^{23}Na transmission, a ^{1}H compatible linear polarized Helmholtz coil (1 Tx ^{23}Na) (Rapid Biomedical GmbH, Würzburg-Rimpar, Germany) was used (distance of the Helmholtz pair = 380 mm, polarization in anterior - posterior direction). For reference, images acquired with a circular polarized double resonant ^{1}H/^{23}Na transceiver head Birdcage coil (commercial 1TxRx ^{1}H/^{23}Na coil, Fig. 1 F) (Rapid Biomedical GmbH, Würzburg-Rimpar, Germany) was used.

Sodium B_1^+ maps were acquired with and without our array using the double angle method [42].

^{1}H imaging: Proton images were acquired using a gradient echo sequence with the following parameters: TE/TR/TA = 10 ms/100 ms/20 s, flip angle = 90°, FoV = 143 × 143 mm^2 (transversal); 220 × 176 mm^2 (sagittal and coronal), resolution = 0.56 × 0.56 × 5 mm^3 (transversal); 0.86 × 0.86 × 5 mm^3 (sagittal and coronal).

For ^{1}H transmission, the systems large-volume birdcage bodycoil was used. A reference measurement was performed using a 12-channel head Rx coil (commercial 12Rx ^{1}H coil, Fig. 1F) (Siemens Healthcare GmbH, Erlangen, Germany) and also the systems transmit coil for ^{1}H transmission.

In order to evaluate parallel imaging performance, g-factors were calculated using the SENSE [43] formalism on the images acquired with the commercial 12Rx ^{1}H coil and with the 8Rx ^{1}H/ 8Rx ^{23}Na coil.

Proton B_1^+ maps were acquired with and without the 8Rx ^{1}H/ 8Rx ^{23}Na coil using the double angle method.

2.3.2. In-vivo

All methods were performed according to the relevant guidelines and regulations. The *in-vivo* head scans were approved by the local Institutional Review Board and acquired with prior written informed consent. *In-vivo* images were acquired of two healthy male volunteers (25 and 29 years old).

^{23}Na imaging: The 3D density adapted radial sequence was used with the following parameters: TE/TR/TA = 0.74 ms/32 ms/6:24 min, flip angle = 48°, FoV = 250 mm, isotropic resolution = 4 × 4 × 4 mm, projections = 12,000. The noise scan for channel combination was performed with the same parameters but with only 1200 projections and no transmit power applied.

^{1}H imaging: Proton images were acquired using a gradient echo sequence with the following parameters: TE/TR/TA = 10 ms/100 ms/20 s, flip angle = 25°, FoV = 220 × 220 mm^2 (transversal); 240 × 192 mm^2 (sagittal and coronal), resolution = 0.86 × 0.86 × 5 mm^3 (transversal); 0.94 × 0.94 × 5 mm^3 (sagittal and coronal).

In order to evaluate the g-factors the same formalism as for the phantom measurements were used. The images were acquired with the commercial 12Rx ^{1}H coil and with the 8Rx ^{1}H/ 8Rx ^{23}Na coil.

3. Results

3.1. Measurement results

3.1.1. Proton trap

The measured reflection and transmission S-parameter of one exemplary proton trap are depicted in Fig. 2A. For the transmission parameter, −0.8 dB at the sodium and −62.4 dB at the proton frequency were achieved. Reflection parameters of −42.6 dB at the sodium frequency and −1.7 dB at the proton frequency were measured.

3.1.2. S-parameter and broadband matching

Coupling between the proton and sodium coil elements was in the worst case −60 dB at the proton frequency (123.2 MHz) and −50 dB at the sodium frequency (32.6 MHz).

^{23}Na array: The decoupling between nearest coil elements was −16.4 ± 2.4 dB (average ± standard deviation, calculated from the dB values), worst case decoupling was −13 dB. Active detuning of the different coil elements was −26.8 ± 1.9 dB (worst case −23 dB). Preamplifier decoupling for the different coil elements was −26.4 ± 3.1 dB (worst case −21 dB).

Highest coupling occurred between the next nearest neighboring coil elements (−14 dB). The loaded Q-factor of the sodium coil elements was 140 (Q-loaded to Q-unloaded ratio = 0.93) which resulted in a reflection factor for the broadband matching of in $r = 0.24$.

^{1}H array: The decoupling between nearest coil elements was −16 ± 3.4 dB (worst case −12.5 dB). Active detuning of the different coil elements was −30.6 ± 3.2 dB (worst case −25 dB). Preamplifier decoupling for the different coil elements was −25.1 ± 4.6 dB (worst case −18 dB).

The coupling between next nearest and nearest coil elements was almost similar (−16 dB). The reflection factor for broadband matching was calculated to be $r = 0.56$ with a loaded Q-factor of 120 (Q-loaded to Q-unloaded ratio = 0.92).

3.1.3. Phantom

The SNR results of the phantom measurements are depicted in Fig. 3. The top row shows the ratios of the SNR maps in the central sagittal, coronal and transversal slice for the 8Rx ^{1}H/ 8Rx ^{23}Na coil

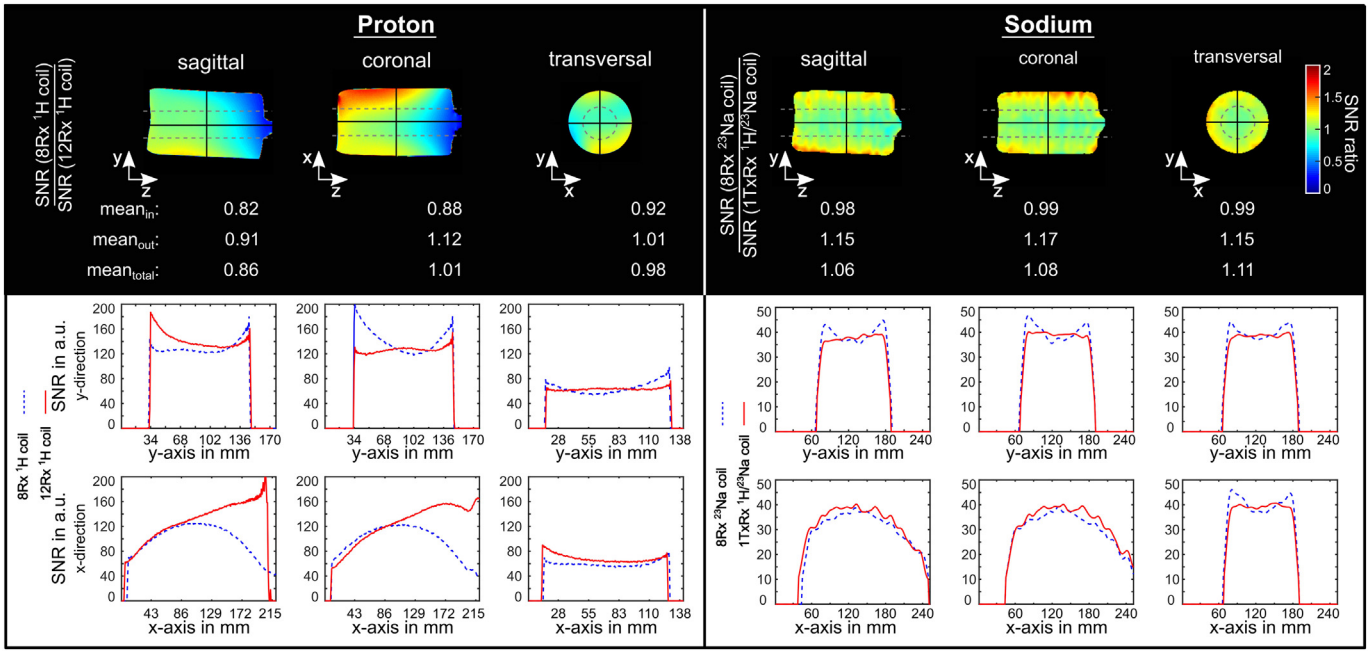

Fig. 3. Top row: SNR ratios in the central sagittal, coronal and transversal slice were calculated for the 8Rx ^{1}H/ 8Rx ^{23}Na coil relative to the reference coils. The gray dotted lines indicate the inner and outer regions of mean SNR calculations. For proton the SNR ratios were, except for the coronal cut, below one. For sodium all ratios were bigger than one. The black lines indicate the positions of the SNR profiles in x- and y-direction. The profiles are plot in the last two rows with the dotted blue line for the 8Rx ^{1}H/ 8Rx ^{23}Na coil and solid red for the reference coils. (For interpretation of the references to colour in this figure legend, the reader is referred to the web version of this article.)

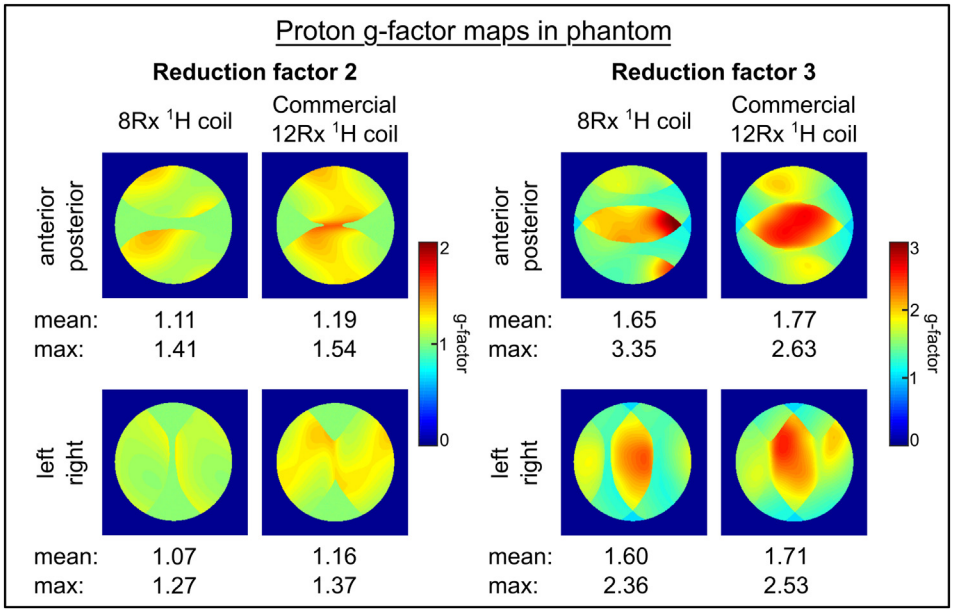

Fig. 4. G-factor maps for proton imaging in the central transversal plane of the phantom measurements for a reduction factor of 2 and 3. The measurements were performed with the 8Rx ^{1}H/ 8Rx ^{23}Na coil and with the commercial 12Rx ^{1}H coil. The g-factor maps were computed in the anterior-posterior and in the left-right direction.

relative to the reference coils (for sodium: commercial 1TxRx ^{1}H/^{23}Na coil, for proton: commercial 12Rx ^{1}H coil).

The mean SNR ratios were evaluated in an inner and an outer region of the phantom as well as in the total image. For the proton measurements the inner SNR mean was between 0.82 and 0.92, the outer mean between 0.91 and 1.12 and the total mean between 0.86 and 1.01. In the sagittal and coronal slices the SNR of the commercial 12Rx ^{1}H coil was higher in the right part of the shown images, which is related to the upper brain region in *in-vivo* applications. This is the case due to the bent structure of the commercial 12Rx ^{1}H coil (Fig. 1 E).

For the sodium measurements the inner SNR mean was between 0.98 and 0.99, the outer mean between 1.15 and 1.17 and the total mean between 1.06 and 1.11.

The profiles of the individual SNR maps in x- and y-direction are given in the last two rows.

The calculated g-factors for the proton measurements are given in Fig. 4. G-factors were computed for reduction factors (R) of 2 and 3 in both phase encoding directions (anterior - posterior (AP) and left - right (LR)). The novel 8Rx ^{1}H coil outperforms the commercial 12Rx ^{1}H coil for each comparison except for the maximum g-factors in anterior-posterior direction with a reduction factor 3.

No g-factors were calculated for the sodium array since due to the low SNR commonly no acceleration is used.

The ratios of the B_1^+ maps for the proton and sodium measurements

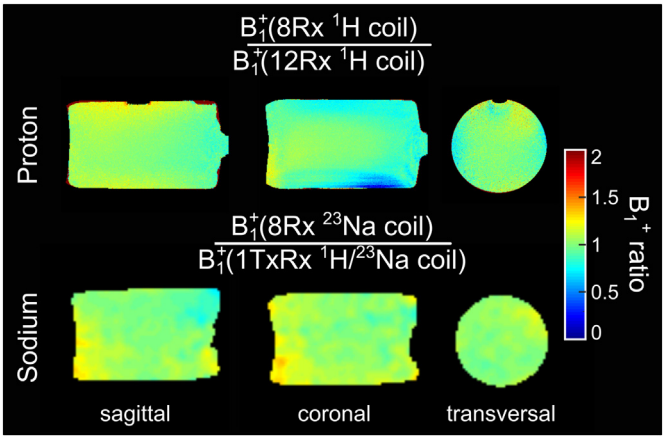

Fig. 5. Ratios of B_1^+ maps in the central sagittal, coronal and transversal plane. The ratios were computed using the B_1^+ maps acquired with the 8Rx ^{1}H/ 8Rx ^{23}Na coil relative to the B_1^+ maps acquired without the 8Rx ^{1}H/ 8Rx ^{23}Na coil.

(ratio with our coil/without our coil) are depicted in Fig. 5. The B_1^+ map ratios of the sodium measurements show minor differences. For the proton measurements higher changes can be detected especially in the coronal direction. Therefore, we lowered the proton specific absorption rate (SAR) limit accordingly.

3.1.4. *In-vivo*

The *in-vivo* SNR measurements in the central sagittal, coronal and transversal slice of the two healthy volunteers (subject 1 and 2) are provided in Fig. 6. The reference SNR maps were acquired for the proton images using the commercial 12Rx ^{1}H coil and for the sodium images the commercial 1TxRx ^{1}H/^{23}Na coil. In case of the proton SNR maps the mean SNR value inside and outside of the marked region are lower for the 8Rx ^{1}H coil. An SNR drop can be seen especially inside the marked region in the sagittal and coronal slices. This is due to the cylindrical shape of the 8Rx ^{1}H coil. The bent shape of the commercial 12Rx ^{1}H coil covers this region of the brain much better. In case of the sodium SNR maps the SNR of the 8Rx ^{23}Na coil are higher compared to the commercial 1TxRx ^{1}H/^{23}Na coil especially in the periphery of the head. This is due to the higher sensitivity of the 8Rx ^{23}Na coil near to the coil elements. The 8Rx ^{23}Na coil also reveals a larger sensitivity region compared to the commercial 1TxRx ^{1}H/^{23}Na coil which can be seen in the neck region in the sagittal and coronal SNR maps.

The *in-vivo* g-factor maps of the two volunteers (subject 1 and 2) in the central transversal slice are given in Fig. 7. G-factors were calculated in anterior-posterior and left-right direction for a reduction factor of 2 and 3. The mean g-factors in case of $R = 2$ are comparable for the 8Rx ^{1}H coil and the commercial 12Rx ^{1}H coil. In case of $R = 3$ the mean as well as the maximum g-factors are higher for the 8Rx ^{1}H coil compared to the commercial 12Rx ^{1}H coil.

The proton performance of the 8Rx ^{1}H/ 8Rx ^{23Na} coil is slightly disadvantageous compared to the commercial 12Rx ^{1}H coil in terms of SNR as well as parallel imaging. In case of sodium the 8Rx ^{1}H/ 8Rx ^{23}Na coil outperforms the commercial 1TxRx ^{1}H/^{23}Na coil. In summary, we achieved complete ^{1}H performance with comparable SNR and parallel imaging performance and enhanced ^{23}Na sensitivity using a single double resonant coil compared to the commercial single resonant coils.

4. Discussion and conclusion

We developed an 8-channel sodium and 8-channel proton double resonant Rx head coil (8Rx ^{1}H/ 8Rx ^{23}Na coil) for MRI at 3T. The combined design of the DGB for the 8Rx ^{23}Na coil and the conventional overlap design for the 8Rx ^{1}H coil was chosen to facilitate the manufacturing process. The 8Rx ^{23}Na coil could be mounted on the coil support without readjusting the dimensions of the array. Decoupling could be simply done using the decoupling capacitors in the 8Rx ^{23}Na coil legs. This was of special benefit to re-adjust decoupling properties after the proton array was mounted on top of the sodium array. Any geometric changes of the 8Rx ^{23}Na coil would have been hard to realize since it was covered by the 8Rx ^{1}H coil. In any case, a realization of the 8Rx ^{1}H coil as a DGB could be also considered.

A possible impact on SNR due to coupling between nearest and next

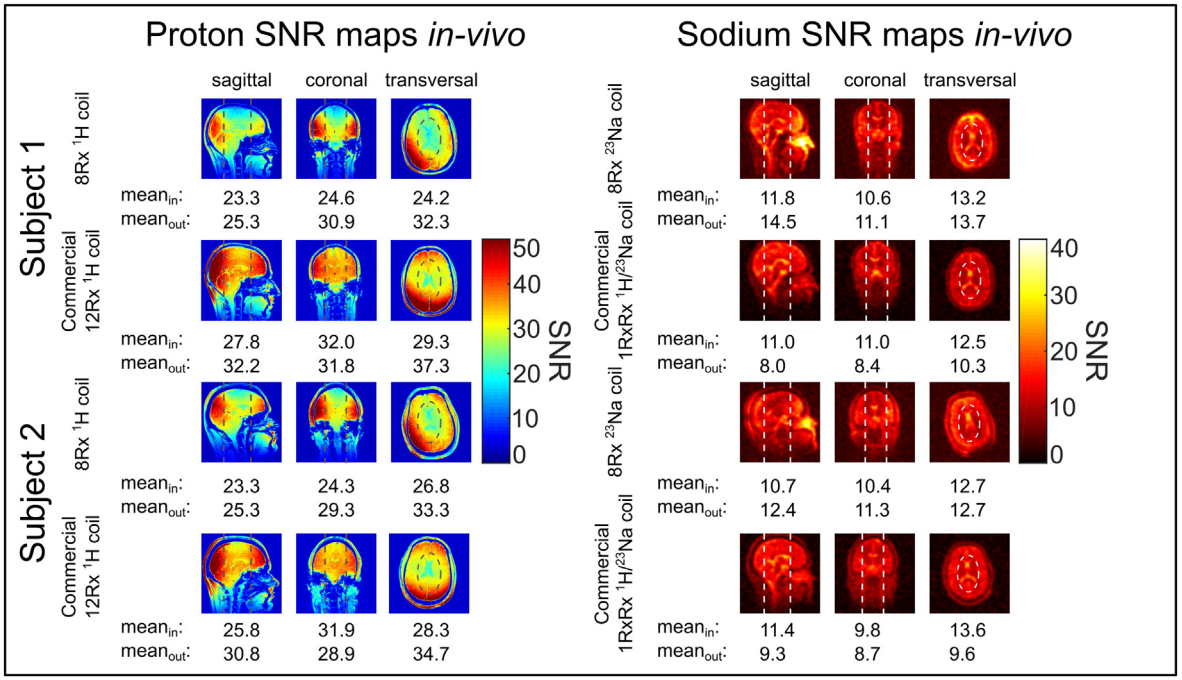

Fig. 6. (Left) *In-vivo* proton and (right) sodium SNR maps in the central sagittal, coronal and transversal plane of the two healthy volunteers (subject 1 and 2). The SNR maps were acquired using the 8Rx ^{1}H/ 8Rx ^{23}Na coil and the reference coils (commercial 12Rx ^{1}H coil for proton imaging and commercial 1TxRx ^{1}H/^{23}Na coil for sodium imaging).

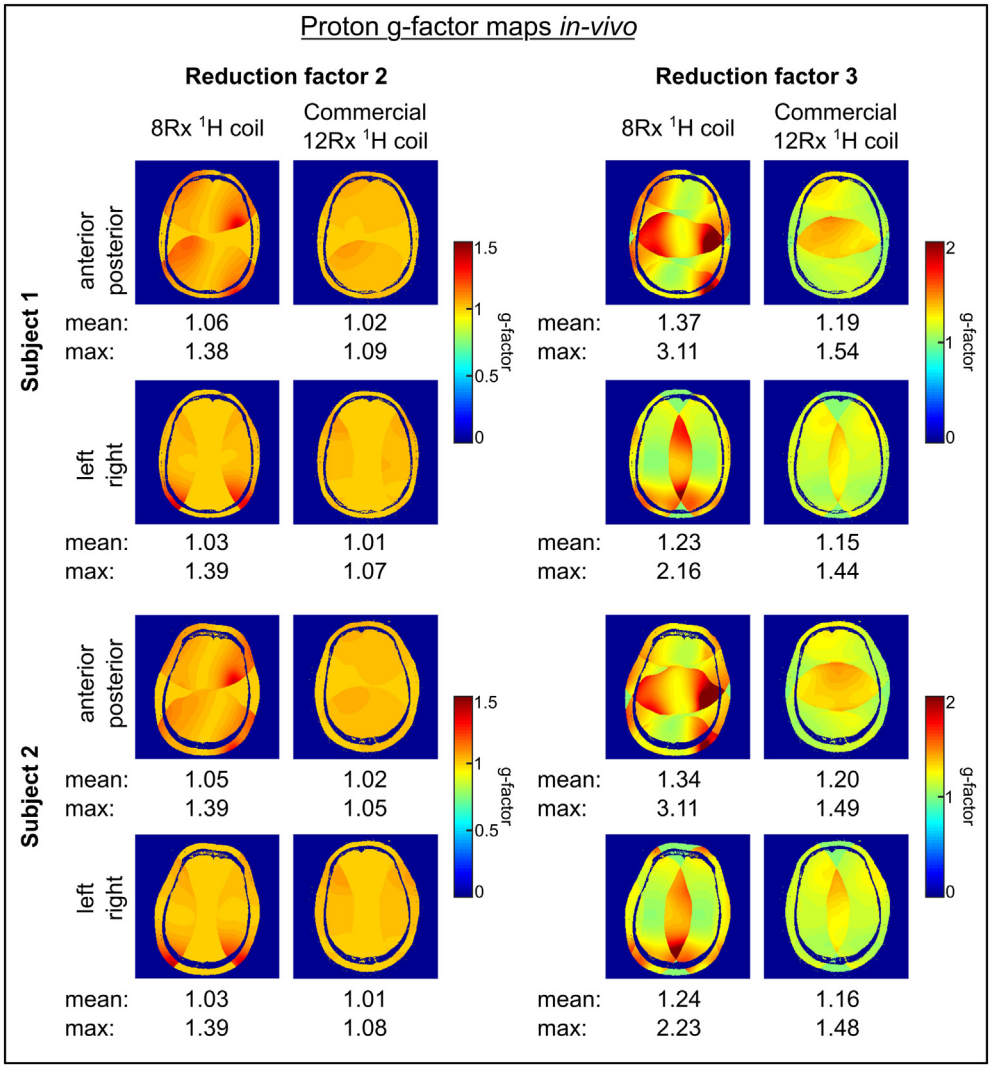

Fig. 7. *In-vivo* proton g-factor maps of the two healthy volunteers (subject 1 and 2) in the central transversal plane for a reduction factor of 2 and 3. The g-factor maps were calculated for the anterior-posterior and left-right direction. The maps were acquired using the 8Rx ^{1}H/ c8Rx ^{23}Na coil and the commercial 12Rx ^{1}H coil.

nearest neighboring coil elements was tried to be avoided by using the broadband matching approach [25,40]. This approach was chosen to avoid additional decoupling circuitry.

Many different designs have been proposed lately for double resonant coil setups. Most often, a nested design has been shown in which the higher frequency coil elements have been placed within the lower frequency coil elements [25,31,32]. These designs have been often realized as transceiver coils for both or at least one nucleus. We did not choose such a design since usually additional transformer decoupling is needed for the inner nested coil elements. This is more complicated to realize and may introduce additional losses. Another point is that the preamplifier cannot be placed directly at the coil element input due to the TxRx switch circuitry which can cause SNR loss. A benefit of the transceiver design is that additional protection fuses are not needed which are necessary for commercial Rx only coils. A fuse is an additional protection during transmission. In case the active detuning circuit fails, the Rx coil becomes off-resonant when the fuse breaks since this opens the coil at the place of the fuse. Such a fuse will add resistance to the coil and decrease SNR. It was found for the nested transceiver setups that no additional trap circuits are needed depending on the distance of the two frequencies under investigation [32]. Such trap circuits are needed to mitigate coupling between coils of difference resonance frequencies. Therefore, the two-staged trap design was selected which presents minimum insertion losses at the resonance frequency with the highest possible impedance at the trap frequency. Due to these traps, no additional proton cable traps were needed for the sodium Rx elements. Nevertheless, three proton traps had to be added to each sodium coil element due to the electrically large DGB structure of the sodium coil. This added up to 2.4 dB losses to each coil element which will also decrease SNR.

In order to compare the performance of the 8Rx ^{1}H/ 8Rx ^{23}Na coil to the commercial solutions we performed phantom and *in-vivo* measurements. In terms of SNR the 8Rx ^{1}H/ 8Rx ^{23}Na coil produced comparable results to the commercial solutions in the phantom measurements. The proton SNR of the 8Rx ^{1}H coil was lower especially in the regions were the design of the commercial 12Rx ^{1}H coil is beneficial due to its bent structure but in the g-factor measurements the coil performances are almost equal. The sodium SNR of the 8Rx ^{23}Na coil was higher, especially in the periphery of the phantom compared to the commercial 1TxRx ^{1}H/^{23}Na coil. In the *in-vivo* measurements again the SNR performance of the 8Rx ^{1}H coil is lower compared to the commercial 12Rx ^{1}H coil especially in the top head region which is due to the bent design of the commercial 12Rx ^{1}H coil. For the g-factor calculations the mean and maximum g-factors of the 8Rx ^{1}H coil were higher compared to the commercial 12Rx ^{1}H coil especially for a reduction factor of 3 which can be explained by the higher coil number of the 12Rx ^{1}H coil which is beneficial for parallel imaging. The sodium *in-vivo* measurements revealed a higher SNR of the 8Rx ^{23}Na coil compared to the commercial

1TxRx $^{1}H/^{23}Na$ coil.

The 1Tx ^{23}Na coil we used for sodium transmission is not optimized for head imaging. We used this coil since we wanted to focus on the Rx only arrays. A dedicated quadrature sodium BC coil for example would be a better choice in terms of homogeneity and transmission efficiency. This suboptimal transmission coil may also be the reason for the SNR drops in some regions of the *in-vivo* measurements. For quantitative sodium MRI the images would have to be corrected for the Rx coil profiles using for example the low-pass [44] or the uniform phantom [45] method.

Finally the B_1^+ field measurements showed a not negligible effect of the 8Rx ^{1}H/ 8Rx ^{23}Na coil on the B_1^+ field especially in the proton case. This might also reduce the SNR performance of the 8Rx ^{1}H/ 8Rx ^{23}Na coil. The SAR limits must be lowered which may increase measurement time for sequences which have a high SAR. In future, field measurements might be a more precise technique to evaluate possible effects on the SAR.

In conclusion, we designed and implemented a double resonant Rx head coil comprised of 8 sodium and 8 proton channels for MRI at 3T. The sodium SNR performance was slightly better than the SNR performance of the commercial 1TxRx $^{1}H/^{23}Na$ coil despite some SNR decrease in the neck region. The proton performance in terms of SNR and parallel imaging performance was comparable to the commercial 12Rx ^{1}H coil. This combination of high sodium sensitivity and full proton imaging capability is believed to make an important contribution towards clinically used sodium MRI due to a more optimized and faster workflow.

References

[1] Madelin G, Lee JS, Regatte RR, Jerschow A. Sodium MRI: methods and applications. Prog Nucl Magn Reson Spectrosc 2014;79:14–47.
[2] Neumann W, Lietzmann F, Schad LR, Zöllner FG. Design of a multimodal (1H/23Na MR/CT) anthropomorphic thorax phantom. Z Med Phys 2017;27(2):124–31.
[3] Platt T, Umathum R, Fiedler TM, Nagel AM, Bitz AK, Maier F, et al. In vivo self-gated 23Na MRI at 7 T using an oval-shaped body resonator. Magn Reson Med 2018;80(3):1005–19.
[4] Wetterling F, Corteville DM, Kalayciyan R, Rennings A, Konstandin S, Nagel AM, et al. Whole body sodium MRI at 3T using an asymmetric birdcage resonator and short echo time sequence: first images of a male volunteer. Phys Med Biol 2012;57(14):4555.
[5] Shah NJ, Worthoff WA, Langen KJ. Imaging of sodium in the brain: a brief review. NMR Biomed 2016;29(2):162–74.
[6] Schepkin VD, Chenevert TL, Kuszpit K, Lee KC, Meyer CR, Johnson TD, et al. Sodium and proton diffusion MRI as biomarkers for early therapeutic response in subcutaneous tumors. Magn Reson Imaging 2006;24(3):273–8.
[7] Schepkin VD, Ross BD, Chenevert TL, Rehemtulla A, Sharma S, Kumar M, et al. Sodium magnetic resonance imaging of chemotherapeutic response in a rat glioma. Magn Reson Med 2005;53(1):85–92.
[8] Thulborn KR, Gindin TS, Davis D, Erb P. Comprehensive MR imaging protocol for stroke management: tissue sodium concentration as a measure of tissue viability in nonhuman primate studies and in clinical studies. Radiology 1999;213(1):156–66.
[9] Thulborn KR, Davis D, Snyder J, Yonas H, Kassam A. Sodium MR imaging of acute and subacute stroke for assessment of tissue viability. Neuroimaging Clin 2005;15(3):639–53.
[10] Neumaier-Probst E, Konstandin S, Ssozi J, Groden C, Hennerici M, Schad LR, et al. A double-tuned 1H/23Na resonator allows 1H-guided 23Na-MRI in ischemic stroke patients in one session. Int J Stroke 2015;10:56–61.
[11] Tsang A, Stobbe RW, Asdaghi N, Hussain MS, Bhagat YA, Beaulieu C, et al. Relationship between sodium intensity and perfusion deficits in acute ischemic stroke. J Magn Reson Imaging 2011;33(1):41–7.
[12] Ouwerkerk R, Bleich KB, Gillen JS, Pomper MG, Bottomley PA. Tissue sodium concentration in human brain tumors as measured with 23Na MR imaging. Radiology 2003;227(2):529–37.
[13] Haneder S, Giordano FA, Konstandin S, Brehmer S, Buesing KA, Schmiedek P, et al. 23 Na-MRI of recurrent glioblastoma multiforme after intraoperative radiotherapy. Neuroradiology 2015;57(3):321–6.
[14] Mellon E, Pilkinton D, Clark C, Elliott M, Witschey W, Borthakur A, et al. Sodium MR imaging detection of mild Alzheimer disease: preliminary study. Am J Neuroradiol 2009;30(5):978–84.
[15] Zostawa J, Adamczyk J, Sowa P, Adamczyk-Sowa M. The influence of sodium on pathophysiology of multiple sclerosis. Neurol Sci 2017;38(3):389–98.
[16] Zaaraoui W, Konstandin S, Audoin B, Nagel AM, Rico A, Malikova I, et al. Distribution of brain sodium accumulation correlates with disability in multiple sclerosis: a cross-sectional 23Na MR imaging study. Radiology 2012;264(3):859–67.
[17] Inglese M, Madelin G, Oesingmann N, Babb J, Wu W, Stoeckel B, et al. Brain tissue sodium concentration in multiple sclerosis: a sodium imaging study at 3 tesla. Brain 2010;133(3):847–57.
[18] Boada FE, Gillen JS, Shen GX, Chang SY, Thulborn KR. Fast three dimensional sodium imaging. Magn Reson Med 1997;37(5):706–15.
[19] Nagel AM, Laun FB, Weber MA, Matthies C, Semmler W, Schad LR. Sodium MRI using a density-adapted 3D radial acquisition technique. Magn Reson Med 2009;62(6):1565–73.
[20] Pipe JG, Zwart NR, Aboussouan EA, Robison RK, Devaraj A, Johnson KO. A new design and rationale for 3D orthogonally oversampled k-space trajectories. Magn Reson Med 2011;66(5):1303–11.
[21] Milford D, Bendszus M, Heiland S. A novel method for T2 quantification in presence of B1 inhomogeneities. Z Med Phys 2018;28(1):63–72.
[22] Niesporek SC, Hoffmann SH, Berger MC, Benkhedah N, Kujawa A, Bachert P, et al. Partial volume correction for in vivo 23Na-MRI data of the human brain. NeuroImage 2015;112:353–63.
[23] Wiggins GC, Brown R, Lakshmanan K. High-performance radiofrequency coils for (23)Na MRI: brain and musculoskeletal applications. NMR Biomed 2016;29(2):96–106.
[24] Barberi EA, Gati JS, Rutt BK, Menon RS. A transmit-only/receive-only (TORO) RF system for high-field MRI/MRS applications. Magn Reson Med 2000;43(2):284–9.
[25] Brown R, Lakshmanan K, Madelin G, Alon L, Chang G, Sodickson DK, et al. A flexible nested sodium and proton coil array with wideband matching for knee cartilage MRI at 3T. Magn Reson Med 2016;76(4):1325–34.
[26] Brown R, Madelin G, Lattanzi R, Chang G, Regatte RR, Sodickson DK, et al. Design of a nested eight-channel sodium and four-channel proton coil for 7T knee imaging. Magn Reson Med 2013;70(1):259–68.
[27] Malzacher M, Kalayciyan R, Konstandin S, Haneder S, Schad LR. Sodium-23 MRI of whole spine at 3 tesla using a 5-channel receive-only phased-array and a whole-body transmit resonator. Z Med Phys 2016;26(1):95–100.
[28] Shajan G, Mirkes C, Buckenmaier K, Hoffmann J, Pohmann R, Scheffler K. Three-layered radio frequency coil arrangement for sodium MRI of the human brain at 9.4 tesla. Magn Reson Med 2016;75(2):906–16.
[29] Ha S, Hamamura MJ, Nalcioglu O, Muftuler LT. A PIN diode controlled dual-tuned MRI RF coil and phased array for multi nuclear imaging. Phys Med Biol 2010;55(9):2589–600.
[30] Han SD, Heo P, Kim HJ, Song H, Kim D, Seo JH, et al. Double-layered dual-tuned RF coil using frequency-selectable PIN-diode control at 7-T MRI. Concepts Magn Reson Part B:e21363.
[31] Lakshmanan K, Brown R, Madelin G, Qian Y, Boada F, Wiggins GC. An eight-channel sodium/proton coil for brain MRI at 3 T. NMR Biomed 2018;31(2).
[32] Brown R, Lakshmanan K, Madelin G, Parasoglou P. A nested phosphorus and proton coil array for brain magnetic resonance imaging and spectroscopy. Neuroimage 2016;124:602–11.
[33] Malzacher M, Chacon-Caldera J, Paschke N, Schad LR. Feasibility study of a double resonant (1H/23Na) abdominal RF setup at 3 T. Z Med Phys 2019https://doi.org/10.1016/j.zemedi.2018.12.004.
[34] Leussler C, Stimma J, Röschmann P. The bandpass birdcage resonator modified as a coil array for simultaneous MR acquisition. Proc Int Soc Magn Reson Med 1997;5:176.
[35] Hayes CE, Edelstein WA, Schenck JF, Mueller OM, Eash M. An efficient, highly homogeneous radiofrequency coil for whole-body NMR imaging at 1.5 T. J Magn Reson 1985;63(3):622–8.
[36] l Mispelter J, Lupu M, Briguet A. NMR probeheads for biophysical and biomedical experiments: Theoretical principles & practical guidelines. Imperial College Press; 2006.
[37] Roemer PB, Edelstein WA, Hayes CE, Souza SP, Mueller OM. The NMR phased array. Magn Reson Med 1990;16(2):192–225.
[38] Vester M, Biber S, Rehner R, Wiggins G, Brown R, Sodickson D. Mitigation of inductive coupling in array coils by wideband port matching. Proc Int Soc Magn Reson Med 2012;20:2690.
[39] Darrasse L, Kassab G. Quick measurement of NMR-coil sensitivity with a dual-loop probe. Rev Sci Instrum 1993;64(7):1841–4.
[40] Malzacher M, Hu R, Chacon-Caldera J, Schad LR. Reducing signal-to-noise ratio degradation due to coil coupling in a receiver array for 35Cl MRI at 9.4 T: a comparison of matching and decoupling strategies. Concepts Magn Reson Part B 2018;48(2):e21383.
[41] Schnell W, Renz W, Vester M, Ermert H. Ultimate signal-to-noise-ratio of surface and body antennas for magnetic resonance imaging. IEEE T Antenn Propag 2000;48(3):418–28.
[42] Cunningham CH, Pauly JM, Nayak KS. Saturated double-angle method for rapid B1+ mapping. Magn Reson Med 2006;55(6):1326–33.
[43] Pruessmann KP, Weiger M, Scheidegger MB, Boesiger P. SENSE: sensitivity encoding for fast MRI. Magn Reson Med 1999;42(5):952–62.
[44] Murakami JW, Hayes CE, Weinberger E. Intensity correction of phased-array surface coil images. Magn Reson Med 1996;35(4):585–90.
[45] Axel L, Costantini J, Listerud J. Intensity correction in surface-coil MR imaging. Am J Roentgenol 1987;148(2):418–20.